EFFECT OF OIL ON FOAM DISPLACEMENTS:

CT COREFLOOD AND DATA FITTING

EFFECT OF OIL ON FOAM DISPLACEMENTS:

CT COREFLOOD AND DATA FITTING

Master Thesis

To obtain the Degree of MSc. in Petroleum Engineering
presented on 29th August 2018.

by

Rayner Vincent D'SILVA

This thesis dissertation has been approved by

Supervisor: Prof. Dr. W. R. Rossen

Thesis Committee:

Prof. Dr. W. R. Rossen	Petroleum Engineering, TU Delft
Dr. A. C. Dieudonné	Geo-Engineering, TU Delft
Dr. D. V. Voskov	Petroleum Engineering, TU Delft
Mr. O. Leeuwenburgh	Senior Research Associate, TU Delft
Mr. J. Tang	PhD Candidate, TU Delft

Dr. Sebastien Vincent-Bonnieu has contributed significantly in realization of this dissertation.

An electronic version of this dissertation is available at
http://repository.tudelft.nl/.

Dedicated to my loving wife

ACKNOWLEDGEMENTS

I would first like to thank my thesis advisors Prof. William.R.Rossen and Dr. Sebastien Vincent-Bonnieu for their continuous guidance and advice. Their involvement and critique in every part of my thesis helped me improve my research and produce satisfying results. I am deeply indebted to them. Next I would like to thank my PhD advisor Mr. Jinyu Tang. The door to Jinyu's office was always open whenever I ran into a trouble spot or had a question about my research or writing. He consistently allowed this thesis to be my own work, but steered me in the right the direction whenever he thought I needed it. I have learned a lot from him.

I want to acknowledge the staff at the Petroleum Engineering faculty who helped me in conducting experiments in a safe manner. They were always present and helpful when some changes had to be made to the experiment setup or any raw materials were required. I also acknowledge all members of the TU Delft Foam group for their advices and ideas with regards to analyzing the experimental data and simulation studies.

I would like to thank Computer Modelling Group (CMG) for their simulator STARS in order to develop my foam model. I would like to express my profound gratitude to all the staff of the CMG customer support group. Without their help and advise I would not have been able to design and run my simulation model. In particular I would like to thank Mr. Marco Misenta, who was my constant contact in the CMG support staff. He was very patient with all of my questions and queries and always tried his best to solve them. I would also like to thank Mr Olwijn Leeuwenburgh who was involved in the optimization of the simulation model. Without his participation and input, the process could not have been conducted.

I express my profound gratitude to all the members of my Thesis defense committee. I appreciate the time they took from their busy schedule and be available for my defense.

Finally, I must express my very profound gratitude to my loving wife for providing me with unfailing support and continuous encouragement throughout the two years of study and through the process of researching and writing this thesis. This accomplishment would not have been possible without her. I would also like to thank my family for all their love and support. Lastly, I would like to thank all my friends and colleagues at TU Delft. It was a great two years of knowing some incredible individuals. Life was much easier studying with you guys.

Thank you.

Rayner Vincent D'Silva.

SUMMARY

Foam is a promising solution for improving the poor sweep efficiency of gas injection for enhanced oil recovery (EOR), in that foam lowers gas mobility significantly by trapping gas bubbles. Most of oils destabilize foam, the effect of which dominates foam strength when foam is in contact with oil and is key to success of foam EOR, but not yet fully understood. This study focuses on understanding oil displacement by foam in lab scale and providing insights for field-scale applications. We carry out the study from two perspectives: a) X-ray CT corefloods that give data on both saturation and pressure response in a foam displacement and b) data fitting to corefloods results.

Experimental studies are conducted with two types of simplified model oil to avoid confusion of the effect of multi-components of crude oil: hexadecane (C16) that is benign to foam and a mixture of C16 and oleic acid that is greatly detrimental to foam stability. CT scanning provides data on oil saturation (So) and distribution along a core during the corefloods. Such key information relates So to foam dynamics as implied by pressure response, in particular foam generation and propagation suggesting efficiency of oil displacement by foam. Specifically, foam is injected in two ways: co-injection of surfactant solution and gas with the intention to generate foam in situ in the presence of oil and injection of pregenerated foam. The co-injection serves to check the effect of oil on foam generation and propagation (anti-foaming effect) in the displacement. The second way investigates de-foaming effect of oil on foam displacement. The results show that foam generation in situ in the presence of oil is possible only when the oil is relatively benign to foam. When oil is very detrimental to foam, the in-situ generation is very difficult even at oil saturation as low as residual oil saturation. The displacement of pregenerated foam with oil consists of two stages of foam propagation due to change in So. Foam drains down So with a weaker strength due to high So in the primary propagation. In the secondary propagation, foam propagates faster with a larger strength, pushing oil forward like a piston.

Fitting coreflood data is then performed using a most widely used local-equilibrium implicit-texture foam model in CMG STARS™ simulator. We propose a fitting guideline for estimating foam simulation parameters based on steady-state foam flow data with oil in a recent study that does not give data on So. The model parameters estimated using this method serve as an initial guess for finding the optimal parameters to fit the coreflood data in simulation. A simulator for foam simulation in STARS is set up for this purpose. A scheme is then developed to optimize the model parameters in fitting the dynamic data. The challenges and difficulties in the fitting are briefly summarized for future work.

CONTENTS

List of Figures

List of Tables

1

INTRODUCTION

1.1. FOAM EOR

Oil production can be done in 3 phases. They are, primary, secondary and tertiary. The tertiary stage or the 'Enhanced Oil Recovery' stage is used as the final step in recovering all the possible crude oil from the reservoir. Injecting gas such as Nitrogen or Carbon Dioxide into oil bearing reservoirs is widely used method in EOR. Injecting gas has some major drawbacks due to its density and viscosity when compared to that of the fluids present in the reservoir. This leads to poor sweep efficiency as the gas contacts and sweeps only a small part of the oil present in the reservoir.

Gravity override and non-homogeneous conditions caused by high permeability are some of the main reasons of poor sweep efficiency of gas. Gravity override is the phenomenon where the lighter fluid flows through the top of the reservoir while the heavier fluid is at the bottom of the reservoir. Higher permeability in individual reservoir layers can cause channeling, where the gas bypasses through various parts of the reservoir when it moves along, creating an uneven or a fingered profile. This channeling causes an inefficient sweep which can lead to missing out on large volumes of recoverable oil in the reservoir.[Lake, 1989]

Foams as described in porous media is a dispersion of gas in liquid such that the liquid phase is interconnected and at least some of the gas flow paths are blocked by lamellae. Or it can be described as the dispersion of a non-wetting phase in a continuous wetting phase, wherein the non-wetting phase is the gas and the wetting phase is the water containing the surfactant. Foams help reduce the gas relative permeability by trapping large amounts of gas. The mobility ratio is much better when compared to a pure gas injection.

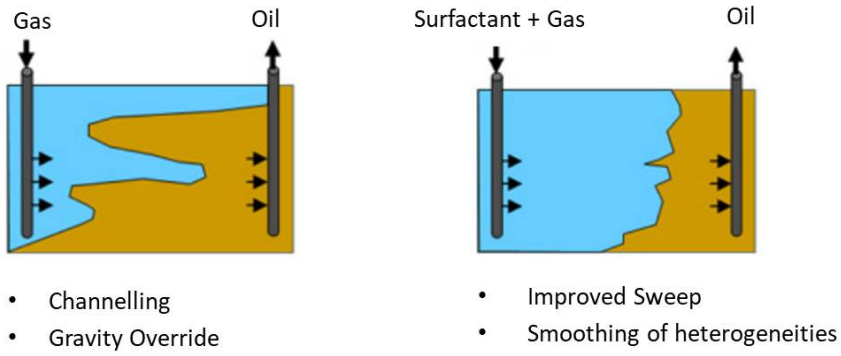

Figure 1.1: Improving Sweep Efficiency using Foam (Source article: The EOR Alliance, 2015).

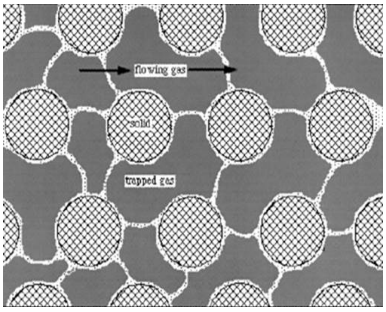

Figure 1.2: Foam in Porous media (Source: Radke and Gillis, 1990).

Foam can help improve this sweep efficiency by reducing the effects of reservoir heterogeneity, viscosity and density.

Foams as described in porous media is a dispersion of gas in liquid such that the liquid phase is interconnected and at least some of the gas flow paths are blocked by lamellae. Or it can be described as the dispersion of a non-wetting phase in a continuous wetting phase, wherein the non-wetting phase is the gas and the wetting phase is the water containing the surfactant. Foams help reduce the gas relative permeability by trapping large amounts of gas. The mobility ratio is much better when compared to a pure gas injection or just gas and water injection without the use of surfactant.

Mobility ratio (M) is defined as the mobility of an injectant (gas) divided by the fluid it is displacing (oil).

$$M = \frac{\frac{k_r g}{\mu_g}}{\frac{k_r o}{\mu_o}}$$

where, krg and kro denotes the relative permeability of gas and oil respectively and μ denotes the phase viscosity. A better mobility ratio helps to produce more oil from the

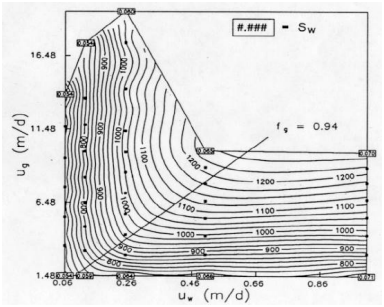

Figure 1.3: Pressure contour plot as a function of gas and liquid flow rates.Region to the upper left of the diagonal line represents the high-quality regime and the region to the lower right of the diagonal represents the low-quality regime. The diagonal line represents the transition between the two regimes and is at a constant foam quality.

reservoir as the problems of channeling; fingering and gravity override are significantly reduced.

The fundamental property of foam flow through porous media is the existence of two flow regimes as in Fig. 1.3: high- and low-quality (gas volume fraction) regimes. These two regimes initially were recognized in the absence of oil. A recent study (Tang et al. 2018) finds that the two flow regimes still apply in the presence of oil but with the vertical contours shifting to the right and horizontal contours moving upward suggesting the destabilizing effect of oil on foam.

Most oils destabilize foam, however, the effect of oil on oil displacement by foam is yet fully understood. This imposes a big challenge to predict and improve the effectiveness of foam processes with oil. This study therefore aims at understanding the impact of oil in the processes of oil displacement by foam in lab scale and provide insights for foam applications in field scale. Specific objectives are described in next section

1.2. OBJECTIVES OF THE THESIS

Foam is very sensitive to various parameters, including oil and water saturation, salinity, reservoir heterogeneity, surfactant composition and concentrations. A foam injection process should be designed in a way such that strong lamellae are produced. The foam generated in the reservoir should be able survive the conditions of that reservoir and also propagate throughout the length of the reservoir. Among other factors, the effectiveness of foam for gas mobility control in presence of oil plays a key role in success of foam EOR. Whether the foam acts as an oil-displacing agent or blocking and diverting agent for the injected displacing fluid, foam generally flows under two types of oil conditions, either directly in contact with flowing oil or at water-flood residual oil.

The interaction of oil with foam is not fully understood. This thesis aims to describe

the foam dynamics under various initial oil conditions. With the help of an experimental setup and the use of a CT scan machine, foam flow dynamics can be observed and studied at water-flood residual oil. Two different oil compositions have been used in this study and the results obtained have been compared to the literatures using different oils, to broaden the understanding of foam flow dynamics in presence of different oil compositions.

The objectives of the thesis can be summarized below:

- Relate oil saturation and type to the efficiency of foam displacement, through their effects on foam generation and propagation in laboratory corefloods.
- Develop an approach for initially estimating foam simulation parameters based on data of steady-state foam flow with oil.
- Set up a simulator in CMG STARS™ for foam simulation.
- Perform foam simulations using conditions the same as in experiments and check the suitability of local equilibrium models for representing dynamic data by comparing simulation and experimental results.
- Summarize difficulties and challenges in fitting foam coreflood data.

2

FOAM THEORY

2.1. OVERVIEW

As discussed briefly in the introduction, steady state foam flow comprises of two regimes

- High-quality regime.
- Low-quality regime.

There are two algorithms in STARS foam simulator for foam flow with oil:

- Wet-foam model where all factors have an impact only on the low-quality regime.
- Dry-out model where all factors have an effect only on the high-quality regime (Tang et al., 2018).

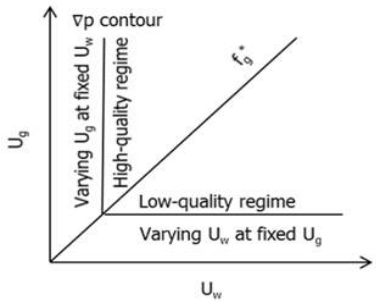

Figure 2.1: Schematic of Δ_p contour in each regime for fitting model parameters to data (Cheng et al. (2000))

2.2. IMPLICIT-TEXTURE FOAM MODELLING

The foam models used in CMG STARS™ falls into 2 categories: 'Population balance' and 'Implicit texture (IT)' models. The population balance models focus on the dynamics of bubble creation and destruction with the gas mobility as a function of the bubble size. The implicit-texture models describe steady-state foam flow assuming local-equilibrium. This study uses a widely used implicit texture model in CMG STARS™. It describes foam strength through a gas mobility reduction factor FM that is a function of a series of factors accounting the effects of water saturation, oil saturation, shear-thinning, salinity, and capillary number. We consider the effect of key factors affecting the efficiency of foam displacement: water saturation, oil saturation, and shear-thinning.(Tang et al., 2018)

$$FM = \frac{1}{(1 + fmmob.F1.F2.F3.F4.F5)} \tag{2.1}$$

where fmmob is the gas mobility reduction factor. This is the maximum attainable gas mobility reduction in the presence of strong foam. The other functions account for the physical factors affecting gas mobility.

Table 2.1: Functions affecting Gas mobility

Function	Variable Description
F1	Surfactant Concentration
F2	Water Saturation
F3	Oil Saturation
F4	Oil Composition
F5	Capillary Number
F6	Salinity

In this study, we consider the effects of water saturation, oil saturation and capillary number using the simulation model in STARS™. Water saturation, which is denoted by F2 in the foam model, is expressed as follows

$$F2 = 0.5 + \frac{arctan(epdry * (Sw - fmdry)}{\pi} \tag{2.2}$$

where epdry regulates the abruptness of foam collapse as the water saturation reduces below the limiting water saturation, which is denoted by fmdry. The effect of oil saturation on foam is denoted by the function F3, which is,

$$F3 = [\frac{(fmoil - S_o)}{(fmoil - floil)}]^{epoil} \tag{2.3}$$

where fmoil and floil are the oil-related parameters marking the boundaries when oil destabilizes and destroys the foam. epoil is the corresponding oil exponent. The shear thinning behavior of foam in the low quality regime is denoted by F5.

$$F5 = (\frac{fmcap}{N_{ca}})^{epcap} \tag{2.4}$$

where fmcap and epcap are the model parameters for shear thinning. Nca is the capillary number and is defined as the product of absolute permeability and pressure gradient divided by water-gas surface tension.

$$N_{ca} = \frac{(k * \Delta_p)}{\sigma_{wg}} \tag{2.5}$$

The factor F2 is denoted as F7 in the dryout model as in this model oil affects gas mobility by limiting the water saturation Sw* (which is called fmdry above and renamed as sfdry in this model) as compared to the wet-foam model which oil alters the fmmob value.

$$F2 = 0.5 + \frac{arctan(sfbet * (Sw - sfdry)}{\pi} \tag{2.6}$$

where sfbet and sfdry are the same as epdry and fmdry in the wet-foam model. The value of sfdry however depends on oil saturation which is as defined by G2.

$$[(1 - sfdry).G2 + sfdry] \rightarrow sfdry \tag{2.7}$$

$$G2 = (\frac{S_o - sloil}{sfoil - sloil})^{efoil} \tag{2.8}$$

where sfoil, sloil and efoil correspond to fmoil, floil and epoil in the wet foam model.

3

EXPERIMENTAL APPROACH

3.1. MATERIALS

3.1.1. CORE SAMPLE

The core used in the experiments was Bentheimer sandstone. It is a very sturdy sandstone and is considered to be consolidated and nearly homogeneous. The core dimensions were 40 cm in length and 4cm in diameter. These core dimensions were cut and milled from a larger block of Bentheimer stone. The core was covered with an epoxy adhesive of Recast CW 2215 + HY 5160. This epoxy adhesive is ideal for casting foundry models and it hardens at room temperature. This epoxy makes it easy to finish and mill after the curing process has taken place. It takes about 48 hours for the epoxy to cure and harden at room temperature. While coating the core with the adhesive it is made sure that no air bubbles are trapped inside the coating. The core coated with the epoxy was then milled as per the dimensions of the core holder used for the experiment. The core holder used in these experiments was made up of polyether-ether-ketone (PEEK), is a colorless organic thermoplastic polymer. It is a synthetic material which displays good mechanical and chemical resistant properties that are retained to high temperatures. It also has a low attenuation of X-rays which makes it ideal to be used for CT scan experiments. Pressure-tap holes were drilled in the core through the epoxy layer along the core length in order to measure the pressure along the core. The connections from the core holder to the apparatus outside were also made of PEEK in order to prevent the pressure lines interfering with the CT scans.

3.1.2. CHEMICALS

The surfactant used in the experiment was the SODIUM C14-16 OLEFIN SULFONATE (BIO-TERGE AS-40, Stepan). It is an anionic surfactant providing excellent viscosity, foam characteristics and mildness. The density of the surfactant is 1.06 g/ml. Sodium Chloride (NaCl, Sigma Aldrich) of 99% purity mixed in de-ionised water (pH = 6.6, Water Lab, TU Delft) was used to provide salinity of 30,000 ppm in all experiments. Normal hexadecane (n-C16, Sigma Aldrich, Reagent Plus) with a purity of 99% and Oleic acid (C18 H34 O2, Fluka Analytical) with a purity of 99 was used as model oils. The density and viscosity of n-C16 measured at 25°C were 0.77 g/cm3 and 3.28 cP, respectively. Similarly, the density and viscosity of Oleic acid measured at 25°C were 0.89 g/cm3 and 40 cP, respectively. 1-Iododododecane (C12H25I, Sigma Aldrich) with a purity of 98% was used as a dopant in order to distinguish between the different phases when scanned by a CT scanner. Nitrogen with a gas purity of 99.98 was used in the experiments. Iso-Propanol (C3H8O, Emplura) and Carbon Dioxide (CO2) were used for cleaning and drying the core after every experiment.

3.1.3. SOLUTION PREPARATION

The surfactant used in the experiments, SODIUM C14-16 OLEFIN SULFONATE, was kept in the oven at 30°C in order to prevent any precipitation. This was done in advance from up to 24 – 48 hours before preparing the surfactant solution. The aqueous solution was prepared by first de-gassing the de-ionised water. Sodium Chloride was then added to it in the ratio of 3wt% The mixture was thoroughly stirred using a magnetic stirrer. When the aqueous mixture was completely mixed and free of any undissolved crystals, the surfactant was then added in the ratio of 0.5wt%. The aqueous solution had the reactivity of 39% and was used for the experiments. Besides using pure normal hexadecane as a model oil, various mixtures of model oils comprising of Oleic acid and hexadecane were also used, in the ratio of 10% by volume of Oleic acid and 20% by volume of Oleic acid. These model oils were also doped with 1-Iododododecane to increase their x-ray absorbance and make them easily distinguishable under the CT scanner when injected with gas and surfactant solution.

3.2. APPARATUS AND EXPERIMENTAL PROCEDURE

3.2.1. THE CT SCANNER

The CT scan images were obtained using the Siemens SOMATOM Definition Dual-energy CT scanner. The X-Ray tube of the scanner operated at dual energies of 80kv and 140kv. The CT scanner makes use of an Ultra-Fast Ceramic (UFC) detector. The thickness of each slice was 2mm and one scan series included 204 images. The B50s filter was used for the reconstruction of the images. Each slice of the image consists of 512 x 512 pixels; and with the Field of View (FoV) of 100 mm the size of each pixel is 0.195 mm x 0.195mm. The CT scanner is considered to be very accurate, as the noise value ranges to

a few Hounsfield units. The core holder was placed on the bed of the scanner horizontally and was supported by a hard polystyrene block which is not affected by the X-rays.

The core holder was placed horizontally on the bed of the scanner. The inlet of the core holder is connected in line with two Vindum Pumps (VP-12K Continuous Pulse-Free High-Pressure Metering Pump). One pump is used for the model oil and the other used for surfactant injection. A gas mass flow controller (Bronkhorst EL-FLOW® SELECT MASS FLOW METERS) was connected in parallel to the system. The outlet of the core holder was connected to and from a back-pressure regulator (50 bars) The effluent line was placed to collect the produced fluids. Nitrogen was supplied using a 200- bar cylinder equipped with a pressure regulator (Swagelok) and connected to the gas mass flow controller. 5 differential pressure taps were drilled in the core and used to record sectional pressure drops across the length of the core. The gap between the core and the core holder is connected with the inlet line to impose confining pressure. A small device was connected between the Vindum pumps and the inlet of the core holder which acted as a pre-generator for foam. A 3-way valve (Swagelok) was connected in line with the pre-generator device in order to allow one to choose between injection of pre-generated foam or switching to injecting the surfactant and gas directly in the core to generate the foam in-situ. The pressure data was recorded by the data acquisition system through LabVIEW. The flow rates from the pumps were measured using computer controlled software (VPware) and a similar gas flow system is used to control the gas outflow from the gas mass flow controller.

3.2.2. EXPERIMENT PROCEDURE

The experimental procedure is as follows. First the core was flushed with Iso-Propanol in order to make sure that there are no residual liquids left behind in the core. Iso-Propanol helps dissolve the oil completely and this helps eliminate any oil or surfactant solution left behind from previous experiments. The oil Vindum pump was used for this purpose. Using the oil pump also make sure that the oil lines will be flushed with the Iso-Propanol making them clean and ready for next use. The core was then flushed with CO2 from a 5-bar gas injection line in order to dry the core. CO2 helps push out all the Iso-Propanol present in the core. The back-pressure regulator can be tweaked slightly to ensure all the Iso-Propanol is pushed out by the CO2. Carbon Dioxide is also highly soluble in water which makes it easier for it to be flushed from the system. Next, the CO2 was pushed out of the core by injecting the core with tap water. The tap water was first degassed in order to remove any gas bubbles present. The water pump was used for this purpose. Again, the back pressure can be raised so that all the CO2 gets dissolved into the water and gets removed from the core. After it is made sure that there is no more carbon dioxide present in the system, a short permeability test is carried out on the core. This permeability test was done by varying the flow rates of the tap water flooding the core. The pressure drop across the core is measured and the corresponding flow rates are known. Applying Darcy's law the permeability across each section can be calculated for a given flow rate. When the permeability was measured, the experiment is continued further. The model oil is then injected into the core using the oil injection pump. The

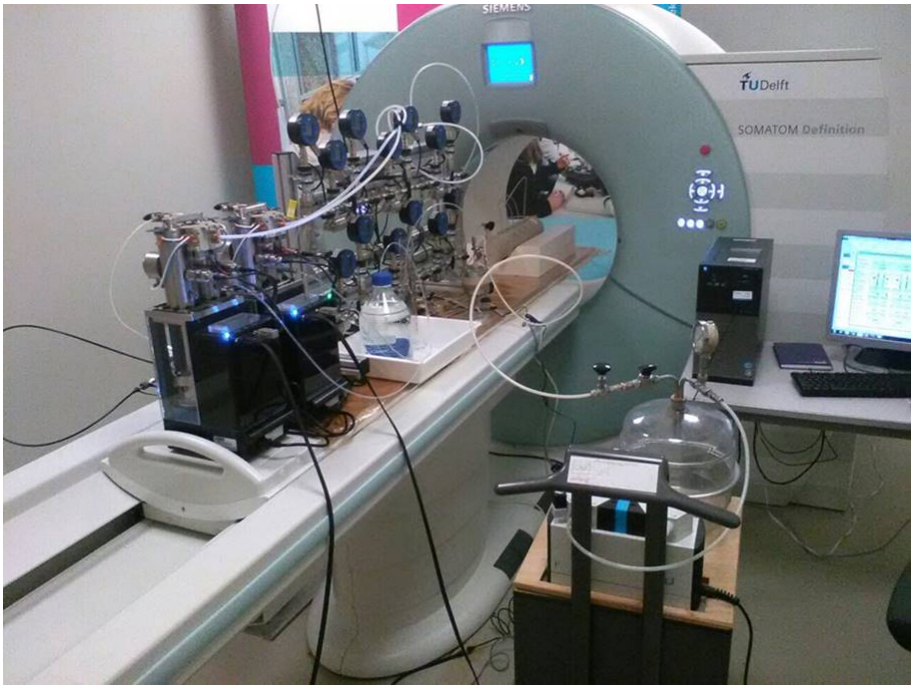

Figure 3.1: Core-Flooding Experiment Setup.

flow rate of oil was maintained at 1.2176 cc/minute throughout all the experiments. The oil is then flooded into the core until connate water saturation is reached. The effluents from the outlet of the core holder are collected and measured in order to estimate the connate water saturation in the core. After the oil flooding is done, the oil line is isolated by a valve and tap water is then injected. The core is then flooded with water to take it to residual oil water saturation. After sufficient water is injected and it is established that the core now is a S_{orw}, the surfactant flooding is then carried out. Around 1PV of AOS solution is injected into the core at a flow rate of 1.2176 cc/minute. This is done in order to quench the surfactant adsorption by the core and to reduce the surfactant loss when flooding the core with foam. Foam flooding is done at a fixed superficial velocity of 4.58 ft. / day with the foam quality of 70%. The back pressure during the foaming flood is maintained at 50 bars.

Two types of foam flooding were carried out.

- The foam was generated in-situ in the core.
- The foam was generated outside using the pre-generator device and the foam was then injected into the core.

The pre-generator is a small device which helps mix the surfactant solution and the ni-

trogen gas to form the foam before it is injected into the core. With the help of a 3 way control valve, which helps us choose the option for the type of foam flooding required in the experiment, the foam formed using this pre-generator device can be injected into the core.

For each experiment, for the different model oil conditions, CT scans of the core was performed to determine the distribution of the fluid saturation in the porous media and to reveal the behavior and propagation of the foam front in the core.

3.3. ANALYSIS OF CT COREFLOOD DATA

3.3.1. 3-PHASE SATURATION CALCULATIONS

The 3-phase saturations can be measured based on the CT measurements. Dual energy is required for the measurement of 3-phase saturation. CT attenuation coefficient is measured for determining the 3-phase saturations. (Welling and Vinegar, 1987 ; Sharma et al, 1997)

The saturations of oil and water are then calculated as follows.

$$So = \frac{[(CTwog)1-(CTw)1][(CTg)2-(CTw)2]-[(CTwog)2-(CTw)2][(CTg)1-(CTw)1]}{[(CTo)1-(CTw)1][(CTg)2-(CTw)2]-[(CTo)2-(CTw)2][(CTg)1-(CTw)1]} \tag{3.1}$$

$$Sg = \frac{[(CTwog)1-(CTw)1][(CTo)2-(CTw)2]-[(CTwog)2-(CTw)2][(CTo)1-(CTw)1]}{[(CTo)2-(CTw)2][(CTg)1-(CTw)1]-[(CTo)1-(CTw)1][(CTg)2-(CTw)2]} \tag{3.2}$$

$$Sw = 1 - So - Sg \tag{3.3}$$

where:
(CTwog)1 = CT attenuation of fluid saturated core at 140 keV, H.U.
(CTwog)2 = CT attenuation of fluid saturated core at 80 keV, H.U.
(CTw)1 = CT attenuation of 100% water saturated core at 140 keV, H.U.
(CTw)2 = CT attenuation of 100% water saturated core at 80 keV, H.U.
(CTg)1 = CT attenuation of dry core at 140 keV, H.U.
(CTg)2 = CT attenuation of dry core at 80 keV, H.U.
(CTo)1 = CT attenuation of 100% oil saturated core at 140 keV, H.U.
(CTo)2 = CT attenuation of 100% oil saturated core at 80 keV, H.U.

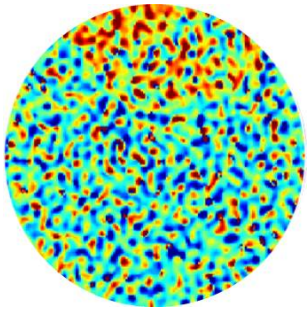

Figure 3.2: CT image slice processed using IMAGEJ FIJI™

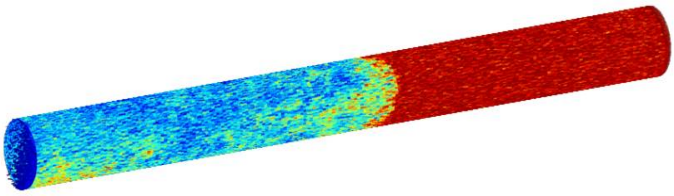

Figure 3.3: Reconstruction of the Core using individual CT Slices

3.3.2. IMAGE PROCESSING

The CT image scans taken during the experimental procedure have to be processed using an image processing software. For the experiments conducted in this thesis, the FIJI™ software by IMAGEJ is used. FIJI™ is an image processing package with useful plug-ins which can be used specifically for scientific image processing.

In this study, 204 CT images were taken during each scan and each slice was processed using the equations in 3.1 , 3.2 and 3.3. The whole core image was then reconstructed back using the image processing software.

4

CT COREFLOOD STUDY OF OIL DISPLACEMENT BY FOAM

4.1. OIL DISPLACEMENT BY FOAM GENERATED IN-SITU

4.1.1. MODEL OIL WITH 20% OLEIC ACID

This experiment was carried out for the model oil of 20% Oleic acid (OA) and 80% Hexadecane (C16). Surfactant solution and nitrogen gas were injected simultaneously in the core to form foam inside the core initially at water-flood residual oil saturation with the model oil above. CT scans were taken during corefloods based on foam response upon injection that is reflected by pressure data monitored via pressure transducers.

Each set of experiments provide 3 sets of data: Pressure drop history for each section that indicates foam response, saturation profile and phase distribution along the core.These data relate oil saturation to foam dynamics, in particular foam generation and propagation that indicates the efficiency of oil displacement by foam.

Pressure response in Figure 4.1 suggests that upon about 50 PV injection there is nearly no foam response except the last section. Initiation of foam response at the last section is thought to be due to capillary end effect (Lake et al.,2014). Backward propagation of foam from downstream to upstream might arise from pressure fluctuations. Whereas in the presence of oil, the propagation is greatly slowed. This means that foam generation in the presence of oil that is greatly detrimental to foam is very difficult. The experimental observations here are contradictory to those with Hexadecane in the study of Simjoo, 2013.

Figures 4.3 to 4.5 shows the CT scans taken at 0.69, 33 and 49.3 PV injection respec-

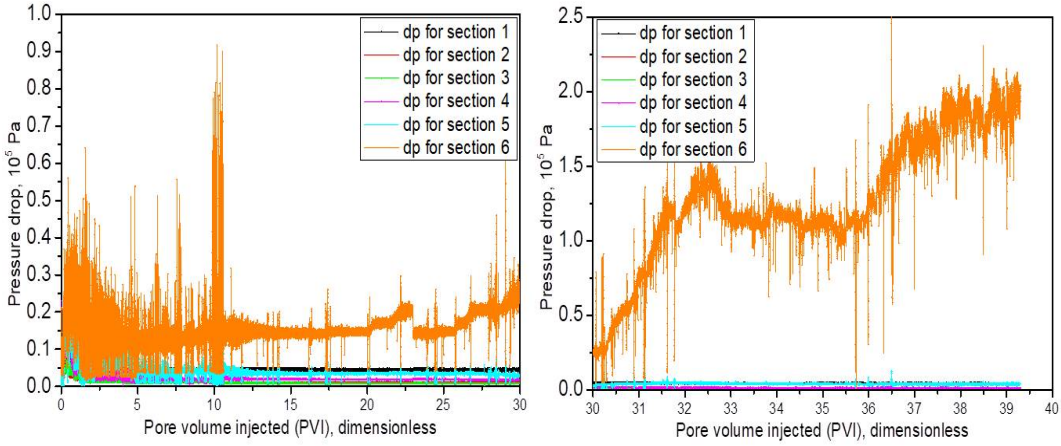

Figure 4.1: Pressure drop profile measured for generation of foam in-situ with 20% OA

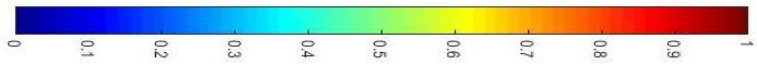

Figure 4.2: Color bar ranging from 0 to 1 representing the value of saturation on the reconstructed CT images of the core

tively, that gives information on saturation profile and phase distribution. Saturation profile in figure 4.3 shows that gas occurs a quick breakthrough and it is water that is displacing the oil ahead upon initial injection. Although pressure data does not indicate foam response in figure 4.1 the phase distribution in figure 4.3 shows that gravity override is mitigated that is also seen in figures 4.4 and 4.5.

In the region near outlet, gas saturation is greater than that of water as shown in figures 4.4 and 4.5. This region grows towards upstream upon injection,another indication for backward foam propagation, that is confirmed by the growth of dark red starting from the end of the core of the gas phase distribution. This is not captured yet in IT foam modelling.

Upon 33 to 49.3 PV injection, oil saturation upstream is as low as residual but there is no noticeable foam response. This challenges the assumption of local equilibrium in IT foam modelling, that foam reaches final state immediately for a given set of saturations.

Saturation profile and pressure drop response together show that, when oil is detrimental to foam, just the presence of oil prohibits foam generation significantly, limiting the efficiency of oil displacement by foam.

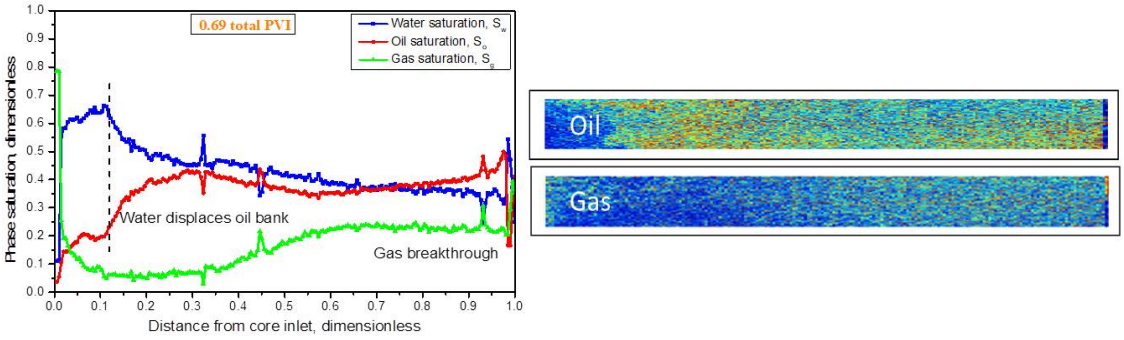

Figure 4.3: Saturation profiles and the reconstructed oil and gas distribution profiles as measured for generation of foam in-situ for 20% OA at 0.69 PVI

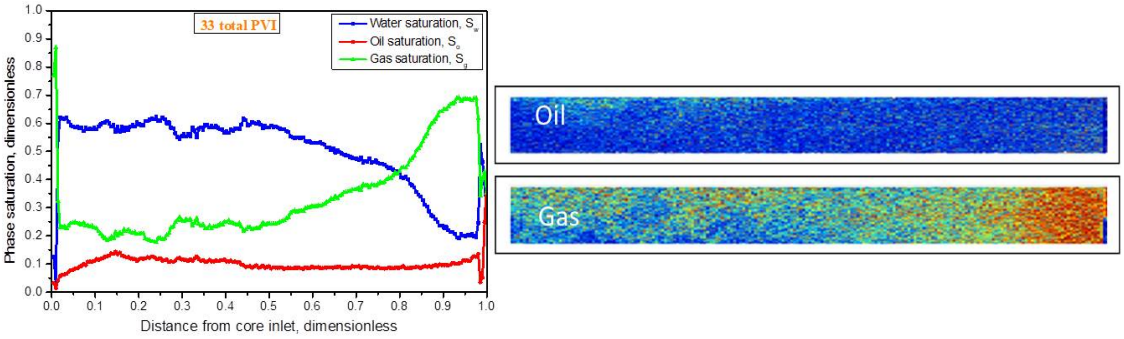

Figure 4.4: Saturation profiles and the reconstructed oil and gas distribution profiles as measured for generation of foam in-situ for 20% OA at 33 PVI

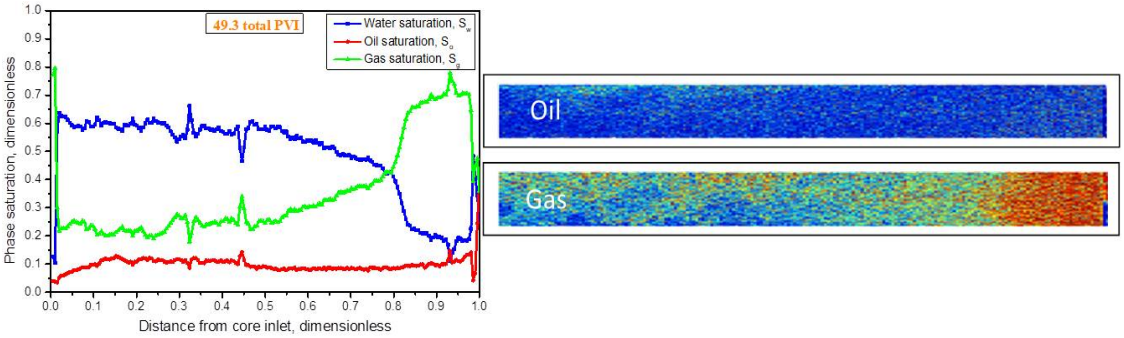

Figure 4.5: Saturation profiles and the reconstructed oil and gas distribution profiles as measured for generation of foam in-situ for 20% OA at 49 PVI

4.1.2. MODEL OIL WITH HEXADECANE (C16)

The effect of Hexadecane on foam when generated in-situ is well documented in the study made by Simjoo and will be used as a reference in this thesis.

As seen in figure 4.6 the region with orange color corresponds to the liquid phase consisting of residual oil plus surfactant solution, two-phase flow region. As gas and surfactant solution are co-injected, the intensity of orange color diminishes progressively in favor of more blue/green, representing the three-phase region. For a longer time of foam injection, figure 4.6 reveals that a new secondary foam front emerges at the downstream of the core and propagates upward against the main flow direction (see the image at 1.0 PV). The appearance of this new front was visualized by a higher intensity of the blue colored zone,indicating that strong foam was generated in the downstream of the core and propagates backwards.This is consistent with the results obtained with the model oil of 20% oleic acid which also shows backward foam propagation as seen in figures 4.4 and 4.5.

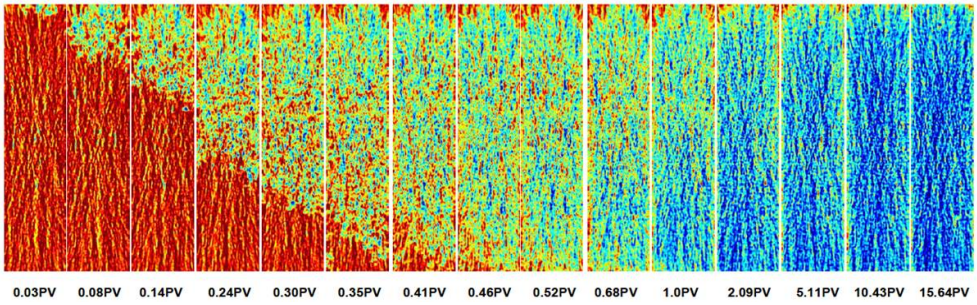

Figure 4.6: CT images obtained during 0.5 wt% AOS foam flooding. Foam breakthrough occurred at 0.41±0.02 PV.(Simjoo, 2012)

Figure 4.7 shows the liquid saturation profiles for the PV of surfactant injected.A high amount of liquid saturation is observed in the inlet region, followed by a reduction inliquid saturation in the upstream region, and then a transition zone through which Sliq increases to unity.

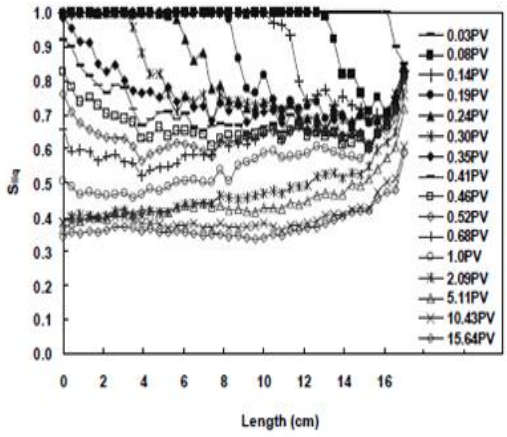

Figure 4.7: Liquid saturation profiles for 0.5 wt% foam obtained from the CT scan images shown in Fig. 4.6.(Simjoo, 2012)

4.2. OIL DISPLACEMENT BY PRE-GENRATED FOAM

4.2.1. MODEL OIL WITH 20% OLEIC ACID

Since foam generation is substantially prohibited by oil components greatly detrimental to foam stability, here we look at the efficiency of oil displacement by pre-generated foam. The results can find applications in a reservoir where foam is generated near well and displaces oil some distance away.

Experimental results provide similarly three types of data:Pressure drop history reflecting foam strength, saturation profile and phase distribution along the core. These three types of data together illustrate the interaction dynamics between foam and oil in porous media, in particular, relating oil saturation to foam dynamics, i.e. foam generation and propagation.

Pressure drop response in figure 4.8 shows that pre-generated foam, under the same conditions, especially the same oil, behaves very differently from foam generated in-situ in an oil displacement process.Generally, experimental observations in figure 4.8 illustrates two stages in foam propagation, both of which move from upstream to downstream. There are two major factors contributing to foam propagation, bubbles newly generated and those accumulated upstream. The prohibition of foam generation in figures 4.1 to 4.5 suggest that foam propagation in figure 4.8 mainly arises from bubble accumulation upstream the speed of which is mainly dominated by oil saturation. Foam, in the primary propagation, displaces oil with less strength than in secondary propagation, in that greater oil saturation destabilizes foam more strongly in the primary stage.

Saturation profiles in figures 4.9 to 4.13 show that it is water that displaces oil ahead in primary propagation. In this stage, most bubbles escape from foam destabilized by

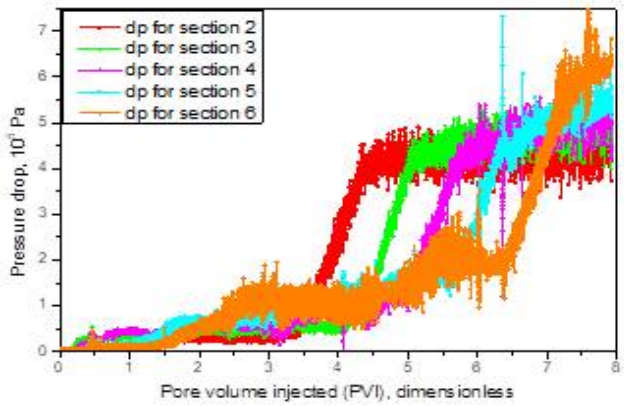

Figure 4.8: Pressure drop profile measured for injection of pre-generated foam with 20% OA

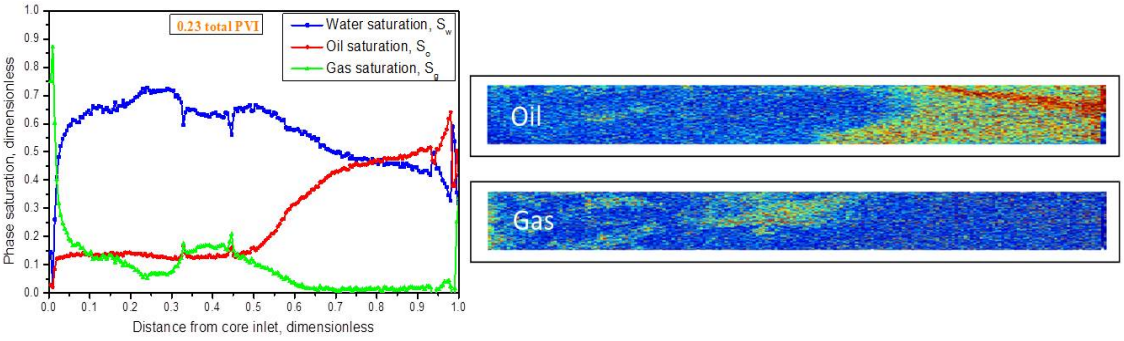

Figure 4.9: Saturation profiles and the reconstructed oil and gas distribution profiles as measured for pre-generated foam with 20% OA at 0.23 PVI

oil with a small portion of bubbles trapped, showing weak foam strength as suggested in figure 4.8. Figures 4.12 and 4.13 demonstrate that foam displaces oil like a piston down to residual in the secondary propagation with larger strengths than the primary due to low oil saturation. This is also illustrated by the piston-like marching front in the gas phase distribution of figures 4.12 and 4.13. Gas phase distribution in figures 4.9 to 4.11 in the primary propagation show that, though without strong foam, a slight reduction in gas mobility could mitigate gravity override.

Additionally, foam propagation yields a retardation in both stages, relative to total amount of fluids injected. For instance, the primary propagation reaches the outflow end upon about 3PV injection. In the absence of oil, foam propagation is limited by surfactant propagation since surfactant is key to stabilize foam. Some studies show that surfactant adsorption could slow down foam propagation. This is not the case in this study since we flush the core with 1PV surfactant solution satisfying surfactant adsorption before foam injection. The reason for slow propagation in the presence of oil is

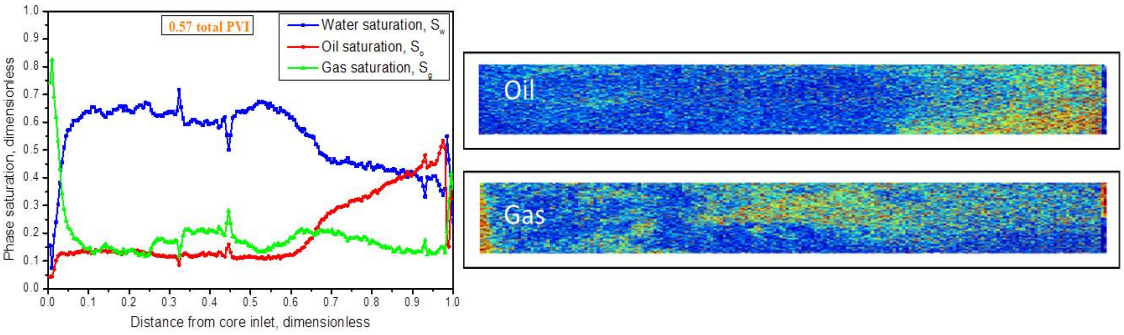

Figure 4.10: Saturation profiles and the reconstructed oil and gas distribution profiles as measured for pre-generated foam with 20% OA at 0.57 PVI

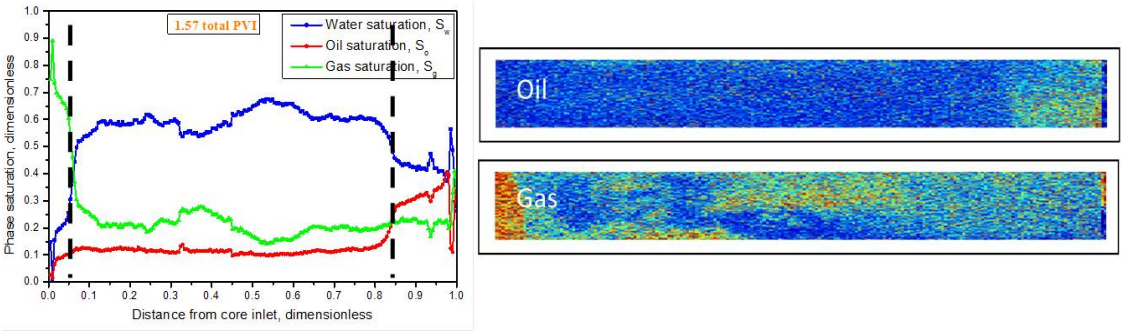

Figure 4.11: Saturation profiles and the reconstructed oil and gas distribution profiles as measured for pre-generated foam with 20% OA at 1.57 PVI

fundamentally not clear yet we think it is the presence of oil that dominates the foam propagation here. Especially the bubbles at the displacement front are more vulnerable to oil that slows down the propagation. More efforts are needed to understand the fundamental reason and improve the current local equilibrium IT foam models to capture these physics. Oil is almost completely stripped near well so that foam could be generated by large velocities and pressure gradients in the vicinity of the injection well. In this case, this type of experimental studies can be used to scale up to the field.

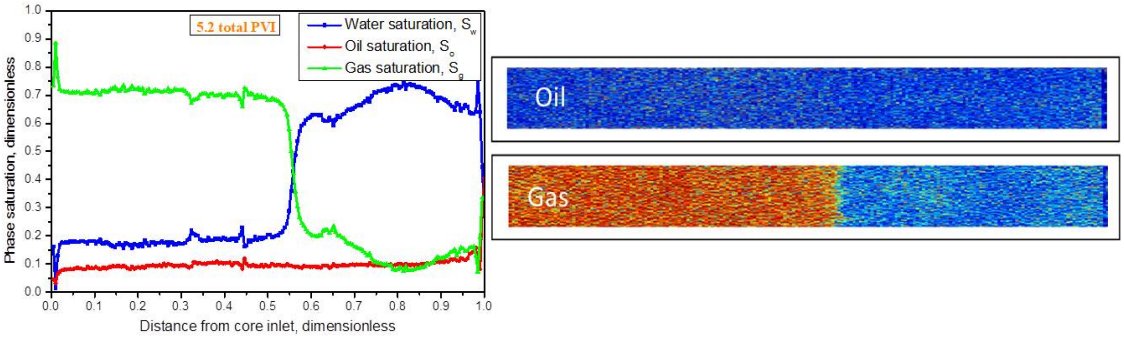

Figure 4.12: Saturation profiles and the reconstructed oil and gas distribution profiles as measured for pre-generated foam with 20% OA at 5.2 PVI

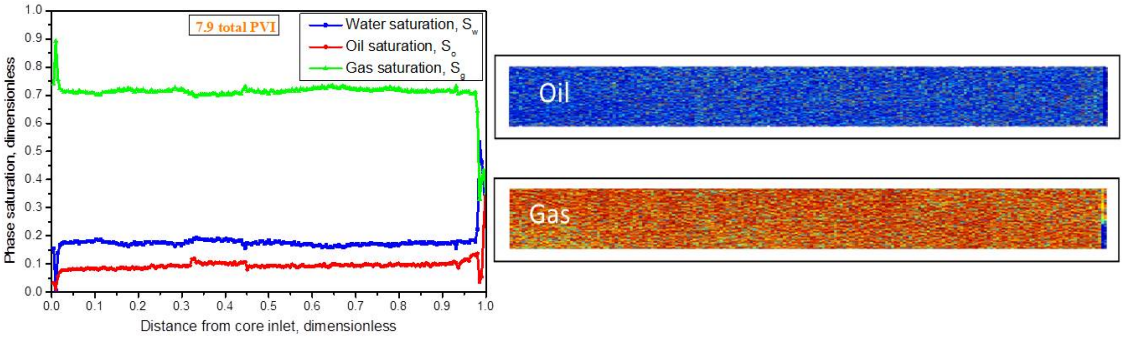

Figure 4.13: Saturation profiles and the reconstructed oil and gas distribution profiles as measured for pre-generated foam with 20% OA at 7.9 PVI

4.2.2. MODEL OIL WITH HEXADECANE (C16)

This experiment was carried out for the model oil of Hexadecane (C16). Surfactant solution and nitrogen gas were mixed outside the core to form a foam and then injected into the core initially at water-flood residual oil saturation. CT scans were taken during corefloods based on the foam response upon injection that is reflected by pressure data monitored vis the pressure transducers. This experiment also provides 3 sets of data:Pressure drop history for each section that indicates foam response, saturation profile and phase distribution along the core.

Pressure drop response in figure 4.14 indicates a very fast foam response. This case also shows two stages of propagation. As observed in figures 4.15 and 4.16.Comparing this to model oil of 20% oleic acid, the primary foam response is much stronger with model oil of C16. This foam front however propagates much slower as it helps to control gas mobility.

With C16, where the oil is not detrimental to foam generation and propagation, foam

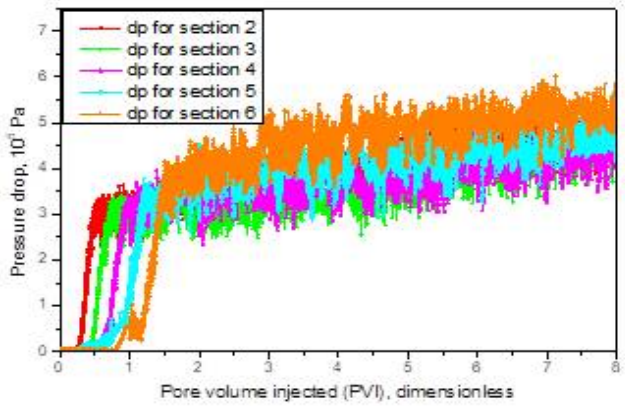

Figure 4.14: Pressure profile measured for injection of pre-generated foam with C16

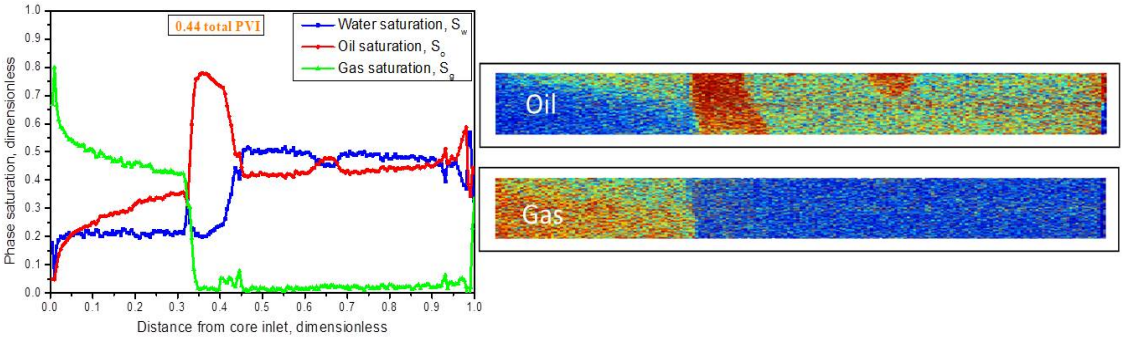

Figure 4.15: Saturation profiles and the reconstructed oil and gas distribution profiles as measured for pre-generated foam with C16 at 0.44 PVI

displaces oil in the primary stage, forming a sharp oil bank as seen in figure 4.15. This is in contrast to what is observed with oleic acid in figures 4.9 and 4.10 where it is water that displaces oil in the primary propagation stage, followed by foam in the secondary propagation stage.The foam displaces oil almost like a piston to residual saturation.

Therefore it can be concluded that Oil type has a huge impact on the displacement mechanisms of pregenerated foam with oil.

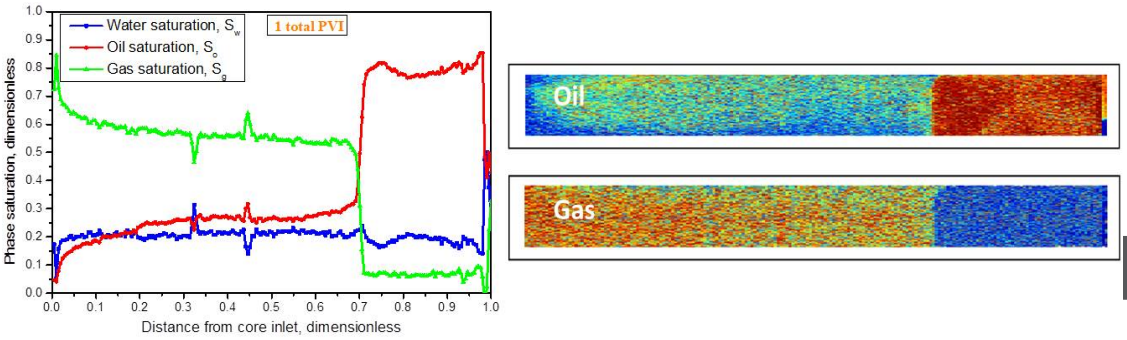

Figure 4.16: Saturation profiles and the reconstructed oil and gas distribution profiles as measured for pre-generated foam with C16 at 1.0 PVI

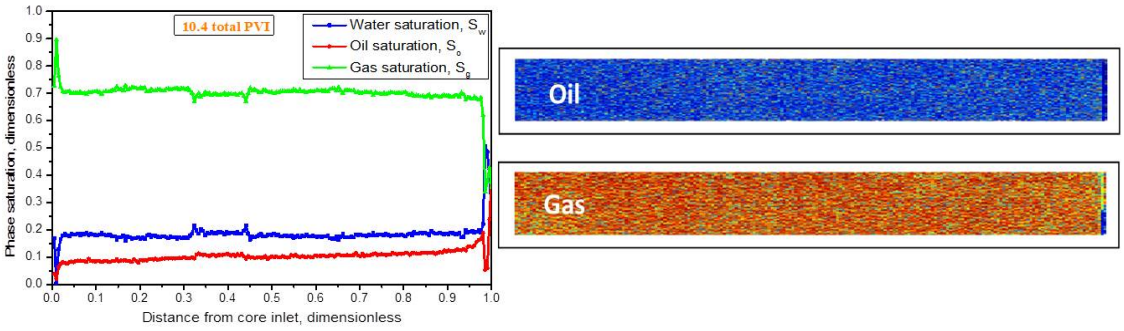

Figure 4.17: Saturation profiles and the reconstructed oil and gas distribution profiles as measured for pre-generated foam with C16 at 10.4 PVI

5

INITIAL ESTIMATION OF FOAM SIMULATION PARAMETERS

Here we propose an indirect approach to fit oil parameters in a widely used IT model based on data of steady-state foam flow with oil that are plotted on a pressure gradient contour plot as a function of gas and water superficial velocities.

It is very important to be able to estimate oil parameters in the high and low quality regime so that its effects on foam behavior can be simulated and studied. In this process we consider the two models,

- Wet-foam model
- Dry-out model

The oil-related parameters which need to be fitted in the two models are:

- fmoil,floil and epoil in the wet foam model
- sfoil,sloil and efoil in the dry out model.

where fmoil and floil are oil related parameters marking the boundary when the oil destabilizes and destroys foam and epoil is the exponent in the wet foam model. The same parameters are renamed as sfoil, sloil and efoil in the dry-out model.

As mentioned in the previous section, in the experiments carried on effect of oil on foam, two model oils were chosen. One was very detrimental to foam generation and propagation (Oleic Acid) and the other was benign to foam (Hexadecane, C16). A study

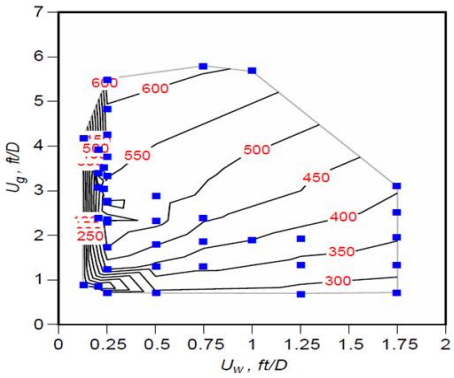

Figure 5.1: Pressure gradient (psi/ft) in the absence of oil, as a function of gas (Ug) and water (Uw) superficial velocities (ft/D) at 35°C in a Benteimer core of 1.98 Darcy. (Source: Jinyu Tang et al.)

conducted by Jinyu Tang et al . performs the same experiments for both the model oils and the pressure gradient in the presence of these oils as a function of gas and water superficial velocities was plotted as shown in figures 5.4 and 5.5. The results of these model oils were compared to that of foam flow without any oil as shown in figure 5.1.

5.1. ESTIMATION OF OIL PARAMETERS IN WET-FOAM MODEL

The following steps can be considered when fitting oil parameters in the wet-foam model.

1. Gas (Ug) and water (Uw) superficial velocities can be determined corresponding to a particular pressure gradient in the low quality regime. These velocities can be calculated since the total superficial velocity is known for the experimental condition, and the ratio of water to oil is always fixed. (Ut = Uo+ Uw+ Ug).These values of Uw and Ug give different points for different pressure gradients in the low-quality regime and can be recorded.

2. The limiting water saturation (Sw*) or (fmdry / sfdry) in the STARS™ model can be calculated based on Darcy's law for the water phase.

$$U_w = \frac{k * k_{rw} * (S_w^*)}{\mu_w} * \Delta_p \tag{5.1}$$

where krw*(Sw*) is calculated based on the Corey Function.

3. Similarly oil saturation can also be determined using Darcy's law for the oil phase

$$U_o = \frac{k * k_{ro} * (S_o^*)}{\mu_o} * \Delta_p \tag{5.2}$$

where kro*(So*) is calculated based on the Corey Function.

4. Since low quality regime is governed by the mobility reduction factor (fmmob), this can be calculated using the relation,

$$U_g = \frac{k * k_{rg}^o * \frac{1}{(1+fmmob*F2*F3*F5)}}{\mu_g} * \Delta_p \tag{5.3}$$

where, krg^o = Gas relative permeability
F2 = Captures the effect of water saturation on gas mobility, which is considered to be 1 in this study.
F3 = Captures the effect of oil saturation and is given by the formula.

$$F_3 = \left(\frac{fmoil - S_o}{fmoil - floil}\right)^{epoil} floil < So < fmoil \tag{5.4}$$

F5 = Captures the shear thinning behaviour which is not considered for 20% OA.

5. Taking in consideration all the known parameters and making simple mathematical arrangements to equation 5.3 we can get the relation ,

$$fmmob * F3 = \left(\frac{\Delta_p * k * k_{rg}^o}{\mu_g * U_g}\right) - 1 \tag{5.5}$$

6. The mobility reduction factor for foam without oil (fmmob*) is given by the following equation

$$fmmob^* = fmmob * F_3 \tag{5.6}$$

The value of fmmob* is already known from the experiment of foam study without oil.

7. Using the relations in equations 5.4,5.6 and 5.6 and simple mathematical rearrangements, the value of fmoil can be calculated for a fixed set of floil and a particular value of epoil for a set of Ug corresponding to a pressure gradient

8. The above steps can be repeated for all the recorded points using the same fixed set of floil values but different epoil values to get a range of fmoil values for that particular epoil.

9. As shown in figure 5.2, for a fixed epoil value there exists an intersection point which gives the best fit of the fmoil and floil values for that particular set of values, specifically the values of fmoil and floil that are consistent with all the horizontal contours as seen in figure 5.1 . Based on this intersection zone, one value of fmoil and floil can be recorded which represents the best-fit values for the steady state data.

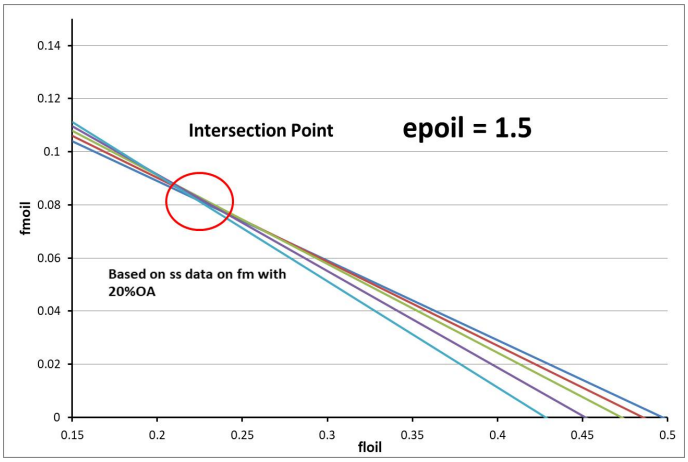

Figure 5.2: Relation between fmoil and floil for a fixed value of epoil

5.2. ESTIMATION OF OIL PARAMETERS IN DRY-OUT MODEL

1. The process of fitting parameters in dry-out model is similar as that of wet-foam model. However the key parameter which needs to be fit here is the limiting water saturation(Sw*).

2. This limiting water saturation is given by,

$$F_7 = 0.5 + arctan\left(\frac{sfbet(S_w^* - sfdry)}{\pi}\right) \tag{5.7}$$

here sfbet = controls the abruptness of foam collapse as water saturation decreases below the limiting water saturation and Sw*.
sfdry = Limiting water saturation which is dependent on the following relation,

$$sfdry = (1 - fmdry) * G_2 + fmdry \tag{5.8}$$

3. The value of fmdry is constant in the high quality regime.G2 is represented by the following relation,

$$G_2 = \left(\frac{S_o - sloil}{sfoil - sloil}\right)^{efoil} \quad sloil < So < sfoil \tag{5.9}$$

4. Limiting water saturation and oil saturation can be calculated using Darcy's law as shown in equations 5.1 and 5.2.

5. Taking in consideration all the known parameters and making simple mathematical arrangements to equation (H) and (I) we can get the relation

$$sloil = \frac{S_o - \left(\frac{sfdry - fmdry}{1 - fmdry}\right)^{1/efoil} + sfoil}{1 - \left(\frac{sfdry - fmdry}{1 - fmdry}\right)^{1/efoil}} \tag{5.10}$$

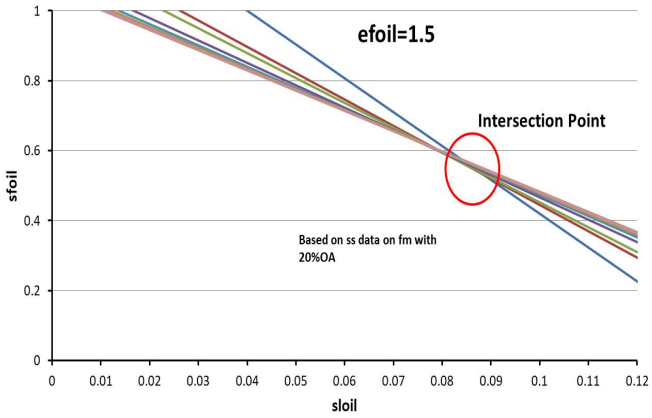

Figure 5.3: Relation between sfoil and sloil for a fixed value of efoil

6. Using the relations in equation 5.10, the value of sloil can be calculated for a fixed set of sfoil and a particular value of efoil for a set of Uw corresponding to the pressure gradients, in figure 5.2

7. The above steps can be repeated for all the recorded points using the same fixed set of sfoil values but different efoil values to get a range of sloil values for that particular epoil.

8. As shown in figure 5.3, for a fixed efoil (1.5 in this case) value there lays an intersection point which gives the best fit of the sfoil and sloil values for that particular set of values. Based on this intersection point, one value of sfoil and sloil can be recorded which represents the best fit values.

5.3. PARAMETER ESTIMATION USING STEADY-STATE FLOW DATA

Two model oils are used for performing the experimental study. 20% oleic acid which is greatly detrimental to foam and Hexadecane which is benign to foam stability. Oleic acid being detrimental to foam exhibits both the regimes and therefore both the dry-out model and the wet-foam model have to be considered when fitting the oil parameters. For fitting the oil parameters with model oil 20% Oleic acid, we can follow the steps mentioned in the equations 5.1 to 5.10

Hexadecane is relatively benign to foam behavior and only wet-foam is considered in this model fit for a constant value of sfdry. Also the shear thinning factor is considered while model fitting for hexadecane.

1. The steps for calculating the oil parameters are the same as used for 20% OA. The same procedure can be followed from equation 5.1 to 5.4.

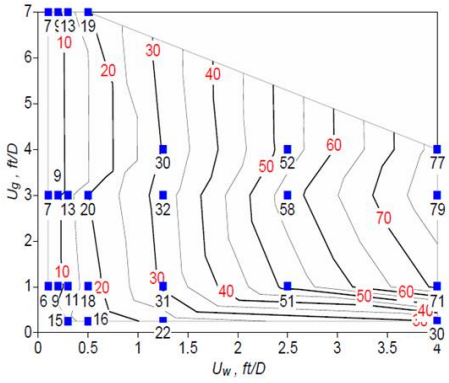

Figure 5.4: Steady-state Pressure gradient (psi/ft) for 20%OA as a function of gas (Ug) and water (Uw) superficial velocities (ft/D) at 35°C in a Benteimer core of 1.98 Darcy. (Source: Jinyu Tang et al.)

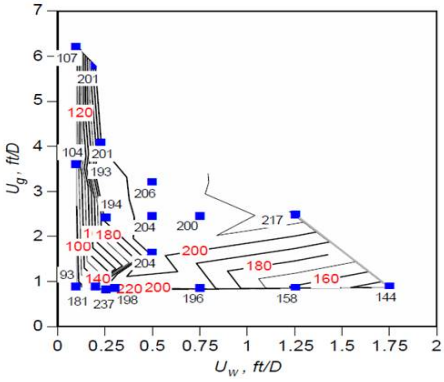

Figure 5.5: Steady-state Pressure gradient (psi/ft) for Hexadecane (C16) as a function of gas (Ug) and water (Uw) superficial velocities (ft/D) at 35°C in a Benteimer core of 1.98 Darcy. (Source: Jinyu Tang et al.)

2. However, in this case the variable F5 is considered and therefore the equation 5.5 is slightly modified as

$$fmmob * F3 = \frac{\frac{\Delta_p * k * k_{rg}^o}{(\mu_g * U_g) - 1}}{F_5} \tag{5.11}$$

where

$$F5 = \left(\frac{fmcap}{N_{ca}}\right)^{epcap}, N_{ca} \geq fmcap \tag{5.12}$$

fmcap and epcap are model parameters for shear thinning effect and Nca is the capillary number.

3. The capillary number is defined by the equation,

$$N_{ca} = \frac{(k * \Delta_p)}{\sigma_{wg}} \tag{5.13}$$

Where σ_{wg} is the water-gas surface tension

4. After working out the solution of equation 5.11, the rest of the steps are similar to the ones carried out in 20% OA from equation 5.6 to 5.10.

5.4. FINDINGS

Result of the fitting of parameters to the Δ_p contour diagrams is that the parameters calculated correspond to an unstable state and it is not something that could be observed in nature.

The issue of unstable states is very complex, and beyond the scope of this thesis, however a good explanation about these unstable states is mentioned in the paper by Jinyu Tang et al.

For the given parameter values that were used for the fit, and the fractional-flows injected in these corefloods, we don't actually get a state that could be observed in nature (or in a simulation).

6

DATA FITTING TO FOAM COREFLOODS

Oil displacement by foam generated in-situ violates the local equilibrium assumption. We perform foam simulation by fitting model parameters to data for oil displacement by pre-generated foam that meets this assumption.

6.1. SIMULATOR SETUP AND PROCEDURE

6.1.1. GENERAL PROPERTIES

Each simulation is set up by creating a 200 x 1 x 1 grid that models the core (Many different grids were tested and 200 grids were chosen as it reduced the inconsistencies caused by purely numerical issues). It is oriented horizontally just like in the experimental setup. Core dimensions, such as the length and diameter of the core as well as initial conditions of the experiment, such as pressure and temperature, water and oil saturation, are used as inputs in the simulation. Moreover, rock properties including porosity, permeability, oil, water and gas viscosity which are constant for each case are also used as inputs.(CMG STARS™ users manual, 2017)

The injection conditions of the oil, water, surfactant solution and gas are mimicked to represent the injection conditions as performed during the experiment. The simulation consisted of 4 injector wells which were used to inject water, surfactant solution, oil and nitrogen gas. The flow rates of the fluids were used as constraints for the injection wells and were the same as the flow rates used in the experiments. The injection times were made to represent the injection times of the laboratory experiments as close as possible. The production well was designed under a constraint of having a bottom

hole pressure equal to the back pressure used in the experiments which was set at 5000 kPa.

The maximum time-step size (dtmax) was chosen as 1 second ($1.15741e-5$ days). This was done in order to note the precise changes in the pressure profiles of the simulation and also to be able to easily compare the output of the simulation to the experimental results as the experimental data as the data capture software used to record the experimental data also used a time step of every 1 second. So also in finite-difference simulations, there are fluctuations in mobility as the foam front advances. These fluctuations are reduced by using smaller grid block size and small time steps for the grid blocks.

Some of the properties that were constant for all the simulation case runs are as follows:

Table 6.1: Experimental Properties

Input	Value	Dimension
Core Length	0.4	metre
Core Diameter	0.04	metre
Temperature	30	°C
Porosity	0.25	
Permeability	1980	mD
Initial water saturation	1	
Water Viscosity	0.7	cP
Oil Viscosity	5	cP
Gas Viscosity	0.0207	cP

6.1.2. ROCK-FLUID PROPERTIES

STARS™ has a function in-built to generate the relative permeability values based on the Corey- Relative permeability correlations.

The Corey functions as calculated by STARS™ are given as

$$Krw = Krwiro * \left(\frac{Sw - Swcrit}{1.0 - Swcrit - Soirw} \right)^{Nw} \tag{6.1}$$

$$Krow = Krocw * \left(\frac{So - Sorw}{1.0 - Swcon - Sorw} \right)^{Now} \tag{6.2}$$

$$Krog = Krogcg * \left(\frac{Sl - Sorg - Swcon}{1.0 - Sgcon - Sorg - Swcon} \right)^{Nog} \tag{6.3}$$

$$Krg = Krgcl * \left(\frac{Sg - Sgcrit}{(1.0 - Sgcrit - Soirg - Swcon} \right)^{Ng} \tag{6.4}$$

Table 6.2: Corey function description as used in STARS™ and the corresponding assigned values

Description	Value Assigned
SWCON - Endpoint Saturation: Connate Water	0.135
SWCRIT - Endpoint Saturation: Critical Water	0.135
SOIRW - Endpoint Saturation: Irreducible Oil for Water-Oil Table	0.1
SORW - Endpoint Saturation: Residual Oil for Water-Oil Table	0.4
SOIRG - Endpoint Saturation: Irreducible Oil for Gas-Liquid Table	0.1
SORG - Endpoint Saturation: Residual Oil for Gas-Liquid Table	0.1
SGCON - Endpoint Saturation: Connate Gas	0.1
SGCRIT - Endpoint Saturation: Critical Gas	0.1
KROCW - Kro at Connate Water	0.5
KRWIRO - Krw at Irreducible Oil	0.713
KRGCL - Krg at Connate Liquid	0.94
Exponent for calculating Krw from KRWIRO	2.46
Exponent for calculating Krow from KROCW	2
Exponent for calculating Krog from KROGCG	1.3
Exponent for calculating Krg from KRGCL	1.3

The Corey relative-permeability values are based on the the relative-permeability data used by Eftekhari and Farajzadeh (2017) for Bentheimer sandstone using same type of surfactant and same concentrations.

Based on the values assigned in 6.2 and experiments conducted in Chapter 4, STARS™ can automatically calculate the water-oil and liquid-gas (Liquid saturation) tables which are used to construct the relative-permeability curves for the numerical simulation.STARS™ uses linear interpolation to smooth out the end points.

Table 6.3: Relative-Permeability table calculated based on the Corey-Parameter values

Relative-Permeability Table					
Water-Oil Table			**Liquid-Gas Table**		
Sw	**Krw**	**Krow**	**Sl**	**Krg**	**Krog**
0.135	0	0.5	0.135	0	0.5
0.164063	0.000778	0.439453	0.164063	0.000778	0.439453
0.193125	0.00428	0.382813	0.193125	0.00428	0.382813
0.222188	0.011606	0.330078	0.222188	0.011606	0.330078
0.25125	0.023552	0.28125	0.25125	0.023552	0.28125
0.280312	0.040778	0.236328	0.280312	0.040778	0.236328
0.309375	0.063857	0.195313	0.309375	0.063857	0.195313
0.338438	0.093303	0.158203	0.338438	0.093303	0.158203
0.3675	0.129585	0.125	0.3675	0.129585	0.125
0.396562	0.173137	0.095703	0.396562	0.173137	0.095703
0.425625	0.224365	0.070313	0.425625	0.224365	0.070313
0.454687	0.283648	0.048828	0.454687	0.283648	0.048828
0.48375	0.35135	0.03125	0.48375	0.35135	0.03125
0.512813	0.427814	0.017578	0.512813	0.427814	0.017578
0.541875	0.513369	0.007813	0.541875	0.513369	0.007813
0.570937	0.608329	0.001953	0.570937	0.608329	0.001953
0.6	0.713	0	0.6	0.713	0

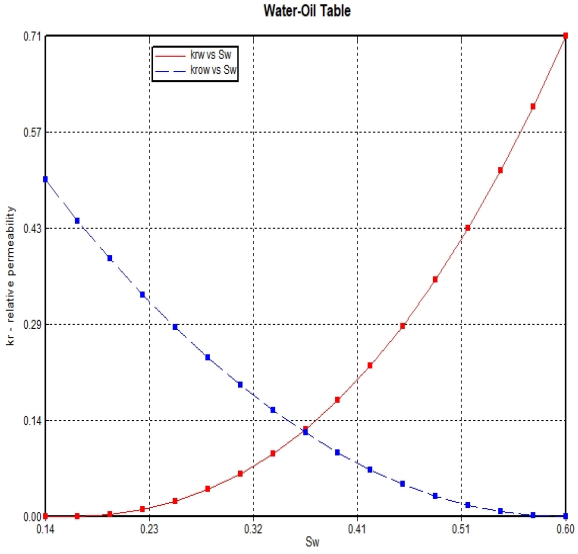

Figure 6.1: Water-Oil relative-permeability values generated by STARS™ using the Corey functions

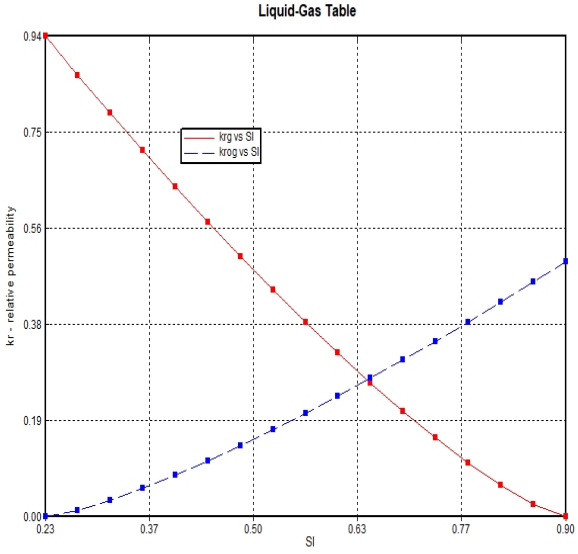

Figure 6.2: Liquid-Gas relative-permeability values generated by STARS™ using the Corey functions

6.2. SIMULATION STRATEGY

The main strategy is to fit the coreflood data using a widely used local equilibrium implicit texture (IT) model in CMG STARS™. The model parameters used in the simulation are estimated based on the steady-state foam flow with oil as shown in chapter 5. Both model oils were tested for the estimated values of the foam parameters and a cariant of those values to try anc compare different test cases. The values of the different test cases tested can be found in tables 6.4 and 6.5 CMG STARS™ was setup in conjunction with MATLAB such that it would generate an ensemble of random values for each of the foam parameters within a specified range and run the simulations automatically. This enabled many simulation runs for varying foam parameters to find the best fit to the experimental data.(Boeije et al ,2013)

6.2.1. FITTING TO DATA WITH 20% OLEIC ACID

As described in section 5.2, since 20% Oleic acid shows the two regimes, both the dry-out and wet-foam model are considered in this model fit.

Table 6.4: Foam parameters used for numerical simulation with 20% Oleic Acid

Foam Parameter	Case 1	Case 2
FMCAP	7.5E-06	7.5E-06
FMMOB	5.99E+06	5.99E+06
SFBET	20000	20000
EPCAP	1.83	1.83
SFDRY	0.146	0.11
FMOIL	0.262	0.8
FLOIL	0.2393	0.05
EPOIL	1.5	1
SFOIL	0.575548	0.8
SLOIL	0.083183	0.05
EFOIL	1.5	1

As seen from figures 6.3 and 6.4 the simulation run for 20% Oleic Acid with the parameters estimated from the model fit as described in case 1 show almost no foam response. The pressure profiles show a negligible change in simulated pressure when compared to the experimental values. The saturation profile shows that even after sufficient injection of surfactant solution and gas, there is no change in the gas saturation profile and it is at a very low value of 0.12

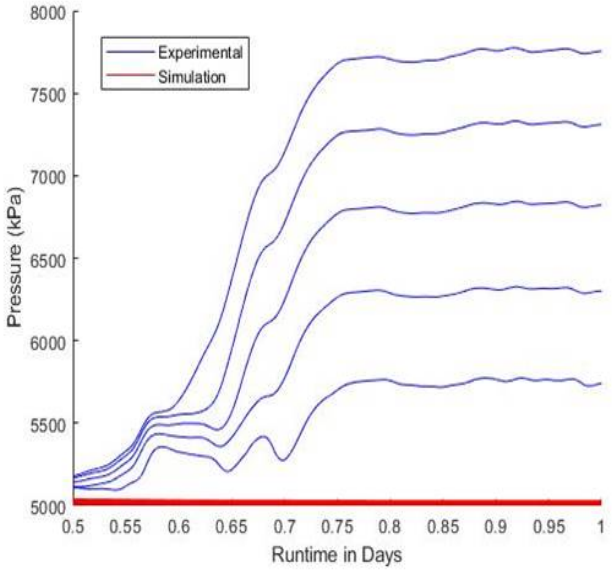

Figure 6.3: Pressure measurement comparison between experimental and simulated data based on the foam parameters for model fit with 20% OA in Case 1 as mentioned in table 6.4

Due to the estimated parameter values not giving a good foam response, the parameter values were altered in a way that a good foam response might be obtained. Foam mobility depends on: fmmob, Oil parameters (fmoil, floil,sfoil,sloil) and sfdry.Since the value of fmmob is already very high in the simulated case, the oil parameter values and the value of sfdry was changed and tested as shown in case 2 on table 6.4

As seen from figure 6.5, the simulation run for 20% Oleic Acid with the parameters described in case 2 did not show any improvement in foam response. The pressure profiles also give a similar result to case 1 , where the foam is not seem to have been generated. Similar test cases were run for varying ranges of sfdry and the oil parameters but without any success.

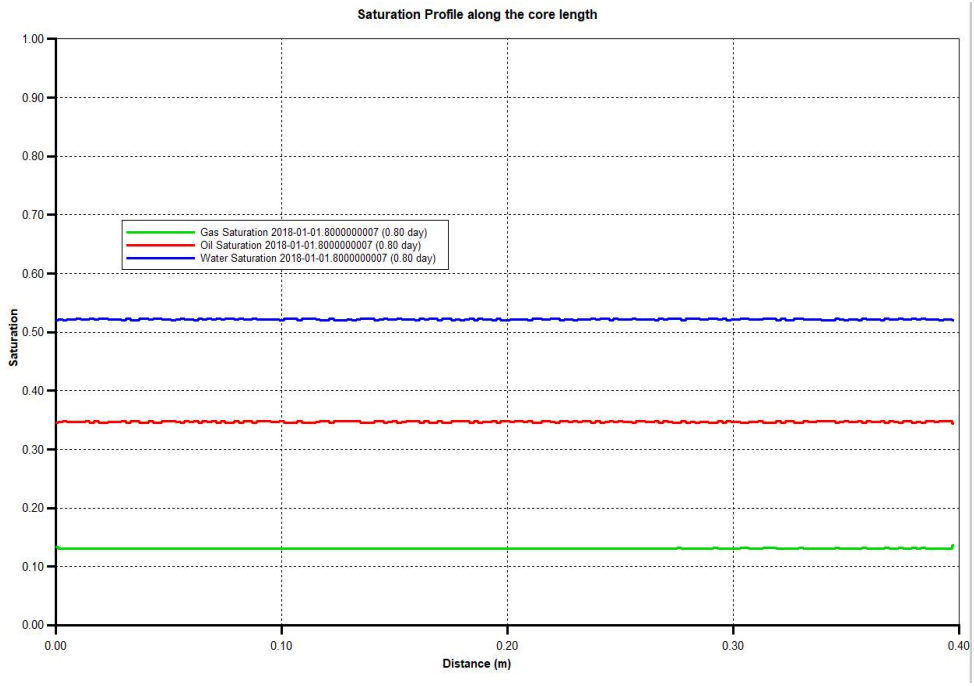

Figure 6.4: Saturation profiles plotted for the simulation parameters for model fit with 20% OA in Case 1 as mentioned in table 6.4.

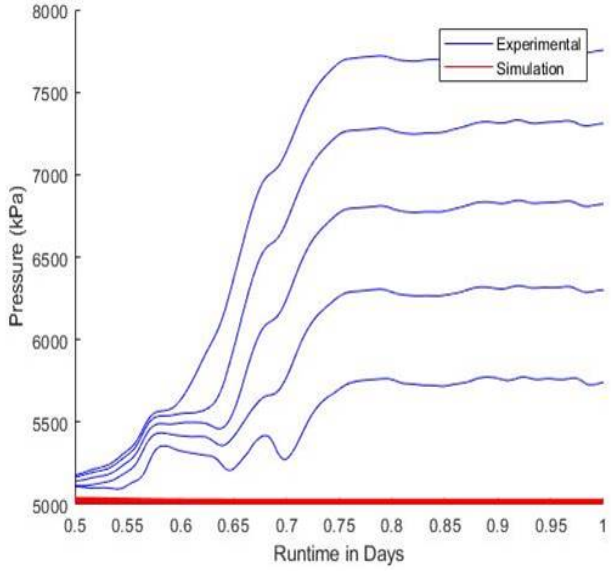

Figure 6.5: Pressure measurement comparison between experimental and simulated data based on the foam parameters for model fit with 20% OA in Case 2 as mentioned in table 6.4.

6.2.2. FITTING TO DATA WITH WITH HEXADECANE (C16)

As described in section 5.2, since hexadecane is relatively benign to foam behavior only wet-foam model is considered in this model fit.

Table 6.5: Foam parameters used for numerical simulation with Hexadecane (C16)

Foam Parameter	Case 1	Case 2	Case 3
FMCAP	7.50E-06	7.50E-06	7.50E-06
FMMOB	5.99E+06	5.99E+06	5.99E+06
SFBET	20000	20000	20000
EPCAP	1.83	1.83	1.83
SFDRY	0.146	0.11	0.11
FMOIL	0.0938	0.8	0.45
FLOIL	0.2857	0.05	0.01
EPOIL	1	1	1

Simulation for C16 for model fit parameters in case 1 as shown in figure 6.6,shows no foam response. This is similar to the case observed in simulation with 20% oleic acid. Similar to the case with oleic acid, the fmoil and floil parameters were altered for the subsequent cases as they control the boundaries when oil destabilizes and destroys foam.

Foam model parameters in Case 3 indicated in table 6.5 also show a similar pressure response where there is negligible pressure increase when compared to the pressure data from the experimental study. The saturation profiles are similar in all the 3 test cases where there is no foam response as indicated by a very low gas saturation value, as low as 0.1.

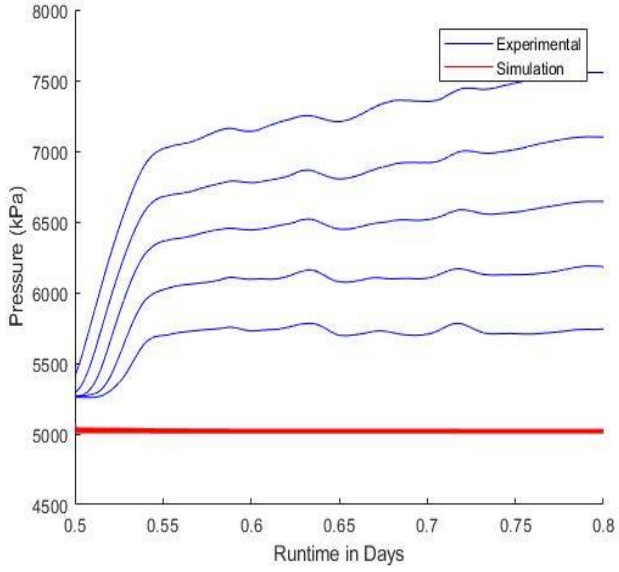

Figure 6.6: Pressure measurement comparison between experimental and simulated data based on the foam parameters in Case 1 as mentioned in table 6.5

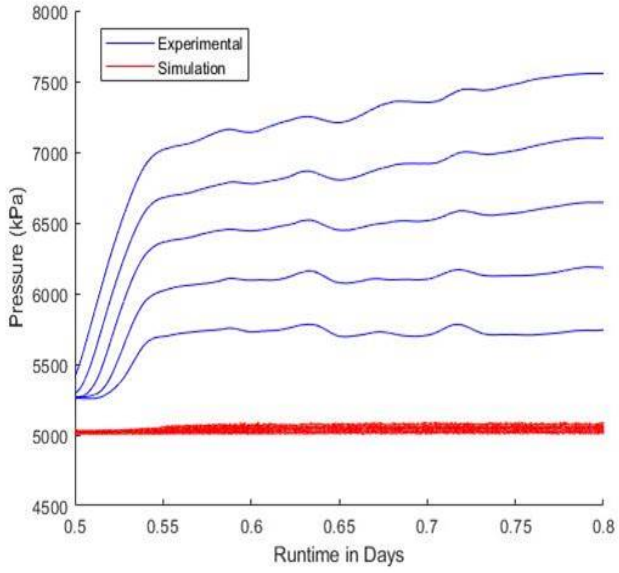

Figure 6.7: Pressure measurement comparison between experimental and simulated data based on the foam parameters in Case 2 as mentioned in table 6.5

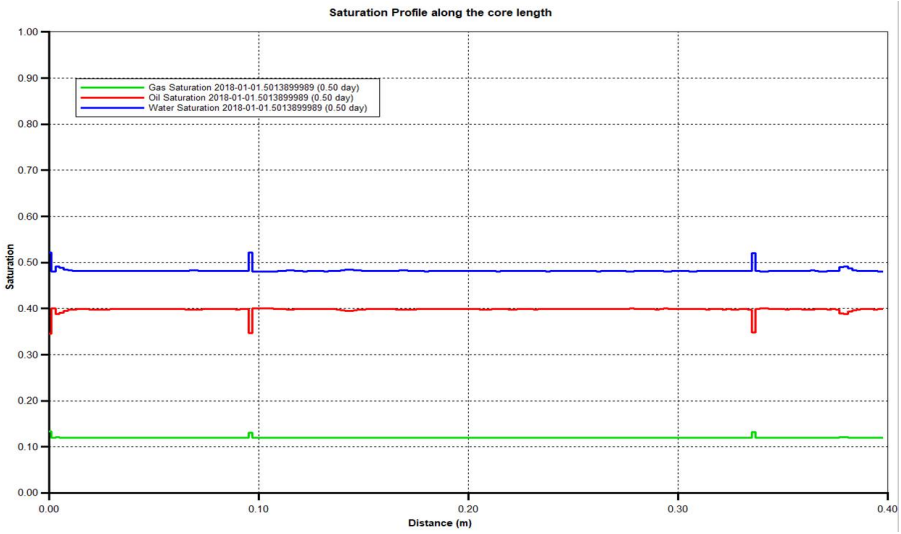

Figure 6.8: Saturation profiles plotted for the simulation parameters for model fit with C16 in Case 1 as mentioned in table 6.5.

6.3. SIMULATION OBSERVATIONS

- As observed from the simulation run for the two model oils , the model foam parameters estimated using the steady state data do not provide a good fit to the experimental data.
- Since there is no foam response for any of the simulation runs and the foam mobility is dependent on fmmob, sfdry and the oil parameters, it is very difficult to estimate which of the parameters need to be adjusted for a given coreflood.
- fmoil and floil affect the low-quality regime only and similarly sfoil ,sloil affect the high-quality regime only. If we are in the other regime with respect to the regime in which we are trying to actually fit the parameters, the estimated parameters will have no effect.
- The reason for the mismatch of simulation data and dynamic coreflood data is not known.It is advisable to test other model foam parameters and also run many simulation studies for variation of the established model parameters in order to get a better match to the dynamic coreflood study.

7

Discussion and Suggestions

The introduction of oil greatly complicates foam flow dynamics in porous media. Experimental observations and data fitting efforts show that fully understanding the process and fundamentals of the effect of oil on oil displacement by foam still faces a number of challenges. In particular, the simulation results do not give a match to experimental observations in our study. The findings raise the concern that one has to be cautious concerning predicting field-scale oil displacement by foam based on laboratory data.

- Experimental observations show significantly different behavior for oil displacement by foam pregenerated or generated in-situ, referred here to as anti-foaming and de-foaming effects of oil. None of current implicit-texture models distinguish these two effects. This means it requires different parameters to fit corefloods data with foam pregenerated or generated in-situ.
- Several physics regarding foam and oil interactions realized in experiment observations are not captured in the current IT foam models. For instance, foam in presence of oil is generated near the outlet and propagates backwards to upstream. Foam propagation shows a retardation relative to total fluids injected either due to surfactant adsorption in the absence of oil or destabilizing effect of oil. Distinguishing the two reasons is a challenge in LE foam modes.
- Fitting a foam model to steady-state data with oil faces a challenge due to the multiple steady-states predicted by the model. In some case we end up with fitting the unstable steady-state to the data.
- All processes related with oil saturation have an uncertainty due to uncertainty in the oil relative-permeability function used. Oil relative-permeability function is affected by whether two-phase or three-phase present, and emulsification of oil seen in our experimental observations.

- Answering the reason for the mismatch between simulation and experimental results is a challenge, given many factors affect the process.

8

CONCLUSIONS

- Oil plays a significantly different role to the efficiency and process of foam displacements, depending on whether foam is generated in-situ or pregenerated.

  For oil displacement by foam generated in-situ:

  - The effect of oil determines the effectiveness of foam displacements. For oils greatly detrimental, foam generation is very difficult, in contrast to that with oil relatively benign, leading to inefficient oil displacement.
  - Foam generation with oil starts near outlet that is thought to be because of capillary end effect occurring at lab scale. Backward propagation towards upstream is due to pressure fluctuations. These phenomena are not captured yet in current IT foam models.

  For oil displacement by pregenerated foam:

  - The flow and transport of foam behaves very differently from foam generated in-situ. Two stages appear in foam propagation dominated by oil saturation (So), both from upstream to downstream. In the primary propagation, most bubbles escape from foam destabilized by oil and few get trapped, with water displacing oil ahead. In the secondary propagation, foam displaces oil like a piston due to So reduced in the primary stage.
  - Laboratory insights for oil displacement by pre-generated foam can be scaled up to the field, in a case where foam is generated near well and displaces oil some distance away.

- An approach is developed to fit oil parameters for foam simulation, based on steady-state data with oil. The anti-foaming effect of oil for foam generation means that different sets of parameters are needed to fit dynamic corefloods with foam pre-generated and generated in-situ.

- Foam simulation with a widely used IT foam model in STARS simulator does not give a match to laboratory data with pregenerated foam. It is a challenge but essential to find the reason for the mismatch, to improve predictability of field-scale foam displacements using lab data. Efforts are needed to develop a method to fit foam simulation parameters automatically to dynamic coreflood data.

REFERENCES

REFERENCES

[1] L Cheng, AB Reme, D Shan, DA Coombe, WR Rossen, et al. Simulating foam processes at high and low foam qualities. In *SPE/DOE improved oil recovery symposium*. Society of Petroleum Engineers, 2000.

[2] R Farajzadeh, M Lotfollahi, AA Eftekhari, WR Rossen, and GJH Hirasaki. Effect of permeability on implicit-texture foam model parameters and the limiting capillary pressure. *Energy & fuels*, 29(5):3011–3018, 2015.

[3] Rouhollah Farajzadeh, Alexey Andrianov, Rumen Krastev, GJ Hirasaki, and William Richard Rossen. Foam–oil interaction in porous media: implications for foam assisted enhanced oil recovery. *Advances in colloid and interface science*, 183:1–13, 2012.

[4] JV Gillis and CJ Radke. A dual-gas tracer technique for determining trapped gas saturation during steady foam flow in porous media. 1990.

[5] Pil-Soo Hahn, TR Ramamohan, and JC Slattery. Mobility control in the displacement of residual oil by an unstable foam. *AIChE journal*, 31(6):1029–1035, 1985.

[6] SA Jones, G Laskaris, S Vincent-Bonnieu, R Farajzadeh, WR Rossen, et al. Surfactant effect on foam: From core flood experiments to implicit-texture foam-model parameters. In *SPE Improved Oil Recovery Conference*. Society of Petroleum Engineers, 2016.

[7] L Kapetas, S Vincent-Bonnieu, R Farajzadeh, AA Eftekhari, SR Mohd-Shafian, RZ Kamarul Bahrim, and WR Rossen. Effect of permeability on foam-model parameters-an integrated approach from coreflood experiments through to foam diversion calculations. In *IOR 2015-18th European Symposium on Improved Oil Recovery*, 2015.

[8] Larry W Lake et al. Enhanced oil recovery. 1989.

[9] Mohammad Lotfollahi, Rouhi Farajzadeh, Mojdeh Delshad, Abdoljalil Varavei, and William R Rossen. Comparison of implicit-texture and population-balance foam models. *Journal of Natural Gas Science and Engineering*, 31:184–197, 2016.

[10] STARS User's Manual. Version 2017.10. *Computer Modelling Group (CMG), Calgary, Alberta, Canada*, 2017.

[11] William Richard Rossen, Christian S Boeije, et al. Fitting foam simulation model parameters for sag foam applications. In *SPE Enhanced Oil Recovery Conference*. Society of Petroleum Engineers, 2013.

[12] WR Rossen et al. Theories of foam mobilization pressure gradient. In *SPE Enhanced Oil Recovery Symposium*. Society of Petroleum Engineers, 1988.

[13] Bakul Chandra Sharma, William E Brigham, Louis M Castanier, and Thomas Reid. *CT imaging techniques for two-phase and three-phase in situ saturation measurements*. PhD thesis, Stanford University, 1997.

[14] M Simjoo, Y Dong, A Andrianov, M Talanana, and PLJ Zitha. Ct scan study of immiscible foam flow in porous media for enhancing oil recovery. *Industrial & Engineering Chemistry Research*, 52(18):6221–6233, 2013.

[15] J Tang, MN Ansari, and WR Rossen. Modelling the effect of oil on foam for eor. In *ECMOR XV-15th European Conference on the Mathematics of Oil Recovery*, 2016.

[16] J Tang, S Vincent Bonnieu, and WR Rossen. The effect of oil on steady-state foam flow regimes in porous media. In *IOR 2017-19th European Symposium on Improved Oil Recovery*, 2017.

[17] Scott L Wellington, Harold J Vinegar, et al. X-ray computerized tomography. *Journal of Petroleum Technology*, 39(08):885–898, 1987.